Numerical simulation of a disk-shaped electron accelerating electrostatic probe

J. H. Nonnast[a] and J. Enoch

Department of Physics and Astronomy, University of Kansas, Lawrence, Kansas 66045

(Received 17 May 1982; accepted for publication 20 October 1982)

This paper presents a method utilizing the numerical plasma simulation particle-in-cell technique for studying electron accelerating probe characteristics. A probe configuration other than the commonly used plane, cylindrical, or spherical case will be studied; the probe configuration used is that of a disk. Cylindrical geometry is used in the simulation model. One of the advantages of a numerical simulation is the ease with which the details of the system can be examined. Therefore, in addition to the current-voltage characteristics of the static probe, other results are presented such as the time evolution of the plasma properties and studies of the sheath region surrounding the probe.

PACS numbers: 52.65. + z, 52.70.Ds

I. INTRODUCTION

The electrostatic probe is a fundamental diagnostic tool which is used to measure properties of a plasma such as density and temperature. Probes are relatively simple devices, but the theory underlying the probe response is extremely complicated. All probe configurations consist of two metallic electrodes in contact with a plasma. The single-probe configuration (used exclusively in this work) consists of a small electrode inserted into the plasma, and a large reference electrode. The single electrode is biased at various positive or negative voltages with respect to the plasma; the current collected by this probe as a function of its potential is measured. This reference electrode, which completes the circuit, is far enough away from the small electrode that it is at the plasma potential. Often this reference electrode is the vessel confining a plasma, or in the case of a satellite-borne system, the body of the satellite. This single probe configuration is described in more detail elsewhere.[1,2]

Electrostatic probe theory is further complicated by the fact that so many different types of plasmas, ranging from partially ionized gases at low pressures to highly ionized gases at high pressures, can be considered. Two basic probe regimes can be identified depending on the ratio of the mean free path of the plasma particles λ to the characteristic probe dimension R. For values of $\lambda/R \gg 1$, the probe is being operated in the collisionless regime. This is the classical Langmuir probe, and it is this regime which is studied in this paper. If $\lambda/R \ll 1$, then collisional effects must be taken into account. This is not considered here.

Probe theory begins with the early work of Irving Langmuir and his collaborators at General Electric Laboratories.[3–5] Langmuir assumed that the plasma surrounding an electric probe can be divided into two distinct regions: a space-charge region or "plasma sheath" which surrounds the probe and which contains all of the potential drop, and a region outside the sheath which is unperturbed by the presence of the probe. A relation which gives the probe current as a function of voltage was obtained for a sheath of finite dimension. Since the current also depended on sheath size (which would have to be determined by experiment) the limit was taken for an infinite Debye length plasma in which the current to the probe is limited by the orbital motions of the particles. Langmuir found that the saturation current for the attracted species varied approximately linearly with voltage for spherical probes and as the square root of the voltage for cylindrical probes. For an infinite plane the saturation current was found to be a constant, independent of voltage. Langmuir assumed that his results were valid for both ion and electron collection by a probe.

Further experiments revealed that the electric field penetrated beyond the sheath edge into the plasma.[6] This new region just outside the sheath is called the quasineutral region or the transition region. Since the mean ion energy in many plasmas is much less than the mean electron energy, even a weak field penetrating outside the sheath region greatly distorts the random thermal motion of the ions. As a result, for an ion-attracting probe, the ions at the sheath boundary can have a directed motion toward the probe which is the same order of magnitude as their thermal velocity.

These results were ignored until the work of Bohm *et al.*[7] They showed that the ion current to a negative probe depends on the electron temperature, because the electron temperature determines the strength of the electric field which accelerates the ions toward the sheath. Therefore, the ion temperature is not easily obtainable from the current-voltage characteristics of an ion-attracting probe. For the one-dimensional case, assuming the electric field at the sheath edge was zero, they showed that an ion velocity of $v_i = (kT_e/m_i)^{1/2}$ was required for a sheath to form. This is now called the Bohm sheath criterion. Allen and Thonemann[8] also arrived at the same result while avoiding the assumption of zero field at the sheath edge.

The Bohm equations are for monoenergetic ions. Allen, Boyd, and Reynolds[9] proved that for a spherical probe, and a Maxwellian velocity distribution in the limit of $T_i/T_e = 0$, the ions will move radially inward, their velocity arising sole-

[a] Present address: Mission Research Corporation, Colorado Springs, Colorado 80907.

 0021-8979/83/020621-11$02.40

ly from the energy they acquire in the potential field of the probe. They also showed that it is not correct to assume for a cylindrical probe that ions start from rest at infinity and move radially inward. Allen, Boyd, and Reynolds were also the first to compute potential distributions in the sheath surrounding a spherical probe.

The first analysis of probe response which includes the full range of particle orbits and the effect of potential barriers was that of Bernstein and Rabinowitz.[10] Monoenergetic ions were assumed, but a completely self-consistent method was used, requiring no separation into a plasma region and a sheath region. A number density for the attracted ions as a function of position and potential was derived for spherical and cylindrical probes. Contrary to what was previously believed, they showed that there is an appreciable dependence on ion energy; ion current could be used to estimate the ion temperature if electron temperature was known.

Lam[11] took advantage of the fact that in many practical cases the ratio of probe radius to Debye length is very large, and used the Bernstein–Rabinowitz model in the asymptotic limit to obtain easy to use current-voltage characteristics for spherical and cylindrical probes. Lam's analysis also provided much insight to the basic structure of the sheath region, the transition region, and the plasma region surrounding the probe. Lam later extended his theory[12] to be valid for moderately large values of probe radius to Debye length.

Laframboise[13] carried out extensive calculations in which Maxwellian velocity distributions were assumed for both ions and electrons. An iterative scheme similar to that of Bernstein and Rabinowitz was used. A trial function was assumed for the charge density near the probe. Poisson's equation was then integrated to yield the electric field. A new charge density was calculated and used with the previous values to obtain a closer approximation to the solution. The completed set of current-voltage characteristics for spherical and cylindrical probes cover essentially the entire range of operation. Hall and Fries[14] used a similar technique to arrive at their own set of current-voltage characteristics for cylinders.

The numerical results of Laframboise are the most accurate set of probe characteristics to date. Because of this, several attempts have been made to obtain formulas which fit these results. Using the numerical solutions of the probe potential distributions of Laframboise along with a theoretical derivation of the current-voltage characteristic given by Kiel and Gustafson[15] fitting formulas have been obtained for cylindrical probe characteristics[16] and for spherical probe characteristics.[17]

Experimental verification of Laframboise's calculations has been carried out by Chen *et al.*[18] They tested cylindrical probes in the orbit-limited regime and spherical probes in the range from $R/\lambda_D = 0$ to $R\lambda_D = 30$. For both types of probes good agreement was found. More recently, Nuhn and Peter[19] used a Ne glow discharge to measure the plasma density with cylindrical probes in the low density region ($0.1 < R/\lambda_D < 0.5$). These experimental results were also found to agree well with the Laframboise results.

Several investigations have been made with probe shapes other than spherical or cylindrical. Laframboise and Parker[20] have removed the restriction of angular momentum conservation used by Langmuir in his orbital-motion-limited theory for spheres and cylinders and rederived the results on the basis of energy considerations alone. They show that any "sufficiently convex" three-dimensional spheroidal collector will collect the same orbit-limited current as a sphere of equal area, and any infinite convex cylinder will collect the same current as a circular cylinder of equal area. Parker and Whipple[21] and Whipple and Parker[22] have examined the circular planar probe in the orbit-limited case and have obtained current-voltage characteristics. These results will be discussed more fully later in this paper.

This paper will present a method utilizing numerical plasma simulation techniques for studying electron accelerating probe characteristics. One of the advantages of a numerical simulation is the ease with which one can examine details of the system being simulated. Therefore, in addition to the current-voltage characteristics of the probe, many other kinds of results will be presented. These include plots of the time evolution of the plasma properties and studies of the sheath region surrounding the probe.

Two probe configurations will be considered separately. The first is that of a "circular planar probe" or a "satellite probe." This consists of a disk-shaped probe which is surrounded in the $z = 0$ plane by an infinite conductor held at zero voltage. This has applications to satellite-borne probes since the infinite plane can be thought of as modeling the satellite skin surrounding a small probe on the top of a cylindrical satellite. This geometry is shown in Fig. 1(a). Probes of this type have been used in several experiments.[23–26] Theoretical studies have also been done[21,27] and simulation results will be compared to these models. Recent studies of pinhole

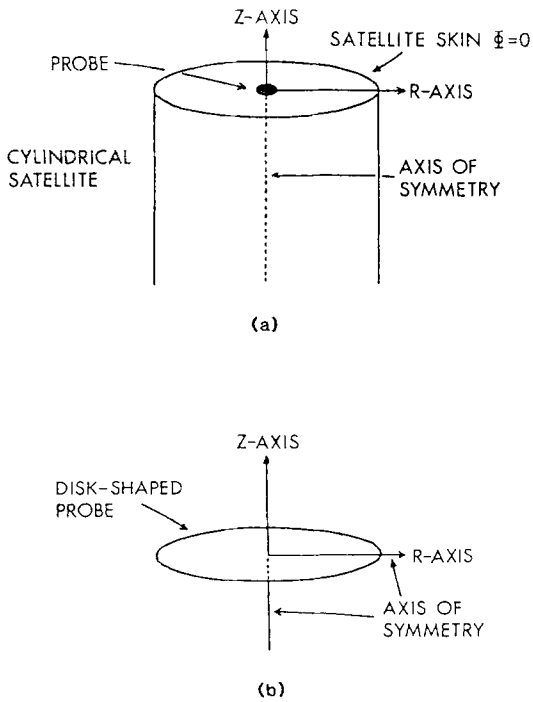

FIG. 1. (a) Circular planar satellite probe. The configuration used in the simulation model takes the satellite skin surrounding the probe to be infinite. (b) Disk-shaped probe configuration.

effects in dielectrics which cover conducting disks held at a negative fixed potential[28–31] can also be compared to the satellite probe configuration. The zero voltage satellite skin can represent a fully charged dielectric, while the probe would represent a hole in the dielectric which exposes the conducting disk to the plasma.

The second configuration which was studied was that of a disk-shaped probe surrounded on all sides by a plasma. The geometry is shown in Fig. 1(b). This configuration would be best described by a disk-shaped probe in a laboratory plasma. This model can be used for comparisons with simulations modeling pinhole effects in dielectrics which cover conducting disks held at a positive fixed potential.[29–31] When secondary emission of electrons from the surface of a dielectric takes place, the dielectric will not become fully charged, and part of the dielectric effectively acts as part of the conductor. The results of the disk-shaped probe configuration can be used to establish an upper limit for current collected by the hole in the dielectric.

Section II will present details of the simulation model for the probe. The characteristics of a circular planar satellite probe are discussed in Sec. III. Section IV describes the results obtained for a disk-shaped probe. Conclusions are given in Sec. V.

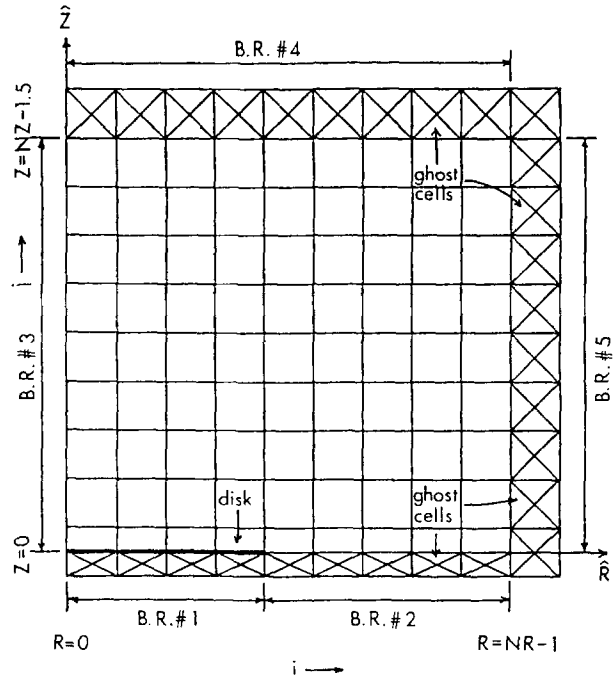

FIG. 2. Calculational grid. The grid size is n_r by n_z and the physical grid size is $n_r - 1$ by $n_z - 1.5$. The five boundary regions are indicated by the abreviation B. R.

II. DETAILS OF THE SIMULATION MODEL

For the simulation of the circular planar electrostatic probe, the particle-in-cell (PIC) method of plasma simulation was chosen. PIC was originally developed by Harlow[32] and others at Los Alamos for use in complicated problems in fluid dynamics. Since then PIC has been refined for use in the simulation of collisionless plasmas.[33–35] The simulation of a circular planar electrostatic probe differs from standard PIC calculations in two major respects. First, in order to take advantage of the azimuthal symmetry of the probe geometry, the present work utilizes a cylindrical coordinate system. This differs from most simulations which use the PIC method in Cartesian coordinates. Thus, most of the techniques in the work are adaptions of standard PIC techniques for a cylindrical coordinate system. Second, standard PIC simulations use either a closed system (that is, a system with physical boundaries) or a system with periodic boundary conditions. In either case, the number of particles in the system is always maintained. Since the probe represents a sink of particles, a closed system is not possible. Thus, the outer boundary of the system is made to be a source of particles where the particles of each species are inserted at each time step at a rate determined by the distribution function of the species distribution at infinity.

Figure 2 is a representation of the calculational grid. The grid size is 32×32, but since PIC requires "ghost" cells at its boundaries, the physical extent of the r axis is from zero to 31 and the extent of the z axis is from zero to 30.5. Boundary region 1 represents the probe. Particles striking this region will be absorbed (that is, removed from the particle arrays in the program). The potential on the grid cell centers will be the effective potential between the probe and the plasma:

$$V_{\text{eff}} = V_{\text{probe}} - V_{\text{plasma}}, \tag{1}$$

where V_{probe} is the potential difference between the probe and the reference probe (assumed to be at infinity), and V_{plasma} is the plasma potential. At boundary region 2, particles can either be reflected or absorbed, depending on the type of system being studied. At boundary region 3, particles which pass through the z axis are reflected due to the azimuthal symmetry of the system. Only particles with zero angular momentum can actually travel through the z axis. Boundary regions 4 and 5 are assumed to lie far enough out in the plasma away from the sheath region that they have zero potential on the grid centers. At each time step, particles are inserted across boundary regions 4 and 5.

The potential is calculated at each time step using point successive overrelaxation (SOR) with odd-even stepping through the grid.[36] Odd-even stepping allows the SOR routine to be put into vectorized form for use on a CRAY-1 computer. This is a self-consistent calculation so that the potential is recalculated every time step.

For the integration of the equations of motion the second-order leap-frog method[34,35] is chosen. It is possible to apply these finite difference formulas using cylindrical geometry.[37] Problems occur, however, when a particle with small angular momentum approaches the z axis. Because the particles are moved in finite steps, the centrifugal force term can become unrealistically large as r goes to zero. One way this can be avoided is to move the particle by an alternate method when it gets too close to the z axis. Another way of avoiding the singularity on the z axis would be to convert to Cartesian coordinates for the particle mover, and then convert back to cylindrical coordinates when the move is completed.[38] This is the method chosen for this simulation.

At the beginning of the simulation run, the plasma ma-

croparticles are spread across the grid area with constant density. The velocities v_r, v_θ, and v_z are chosen from the Maxwellian velocity distribution:

$$f(v_r) = f(v_\theta) = f(v_z) = \left(\frac{m}{2\pi kT}\right)^{1/2} \exp\left(-\frac{v_{r,\theta,z}^2}{v_{th}^2}\right), \quad (2)$$

where

$$v_{th} = \left(\frac{2kT}{m}\right)^{1/2}. \quad (3)$$

After each time step, particles are injected across the outer boundaries of the grid. Since the potential on the outer grid boundary is fixed at zero, particles enter at a rate determined by their thermal motions. Because particles will have a greater probability of crossing a boundary surface if their velocities are high, the distribution function which describes their velocities normal to a boundary surface is

$$g(v_r) = g(v_z) = \left(\frac{m}{2\pi kT}\right)^{1/2} v_{r,z} \exp\left(-\frac{v_{r,z}^2}{v_{th}^2}\right). \quad (4)$$

In other respects, the simulation relies on well-tested PIC methods. It should be noted that the PIC method is inherently limited to moderately large plasma Debye lengths. In all calculations presented in this paper, the ratio of the Debye length to the cell size is greater than one. This insures that Debye shielding in the simulation model is the same as for a real plasma.[39]

A disadvantage of a numerical plasma simulation which uses PIC techniques is that the use of a realistic ion mass is not feasible. This is because a realistic mass ratio m_i/m_e will dramatically increase computer run time because of the slower ion dynamics. For the simulation runs described in the paper, ion mass should not play an important role in the results for two reasons. First, when constructing current-voltage characteristics, only the electron current to the probe will be considered. With a mass ratio of one at low positive probe voltages, many ions will also reach the probe because of their thermal energy. This would result in a value for the total current that is less than the electron current. But for realistic ion to electron mass ratios, the ions would reach the probe at a much slower rate. Additional test runs of the simulation model have shown that the ion current would be negligible when compared to the electron current for positive applied voltages greater than $e\phi/kT_i = 1$, where ϕ is the probe potential, and kT_i is the ion temperature in eV. Thus, ion current to the probe will be ignored. A second reason that ion mass should not play an important role in the results is that it is an equilibrium state which produces these results. It does not matter how fast the ions reach this equilibrium state, but simply that the state exists. This reasoning was tested by comparing current-voltage characteristics from three runs, using mass ratios of 1, 4, and 16. No appreciable difference was found. Thus, the current-voltage characteristics shown in this paper can be assumed valid for large mass ratios, but were run with a mass ratio of one.

III. CHARACTERISTICS OF A CIRCULAR PLANAR SATELLITE PROBE

In all of the simulation runs, the outer boundary of the grid is assumed to be far enough away from the sheath region surrounding the probe that the potential can be taken to be zero there. Thus, one of the first considerations is to establish a suitable grid to disk ratio, hereafter designated by G. G is defined to be the extent of the grid in the r direction (in all cases this is equal to 32 grid cells) divided by the radius of the disk.

Typical simulation results are given in Fig. 3. This is a plot of the current drawn by the probe versus the voltage applied to the probe. The current is normalized to the electron current drawn by the probe at zero voltage. Three current-voltage characteristics are plotted for values of G equal to 2, 4, and 5.33.

The characteristic corresponding to $G = 2$ is saturating at the higher voltages. This saturation is not due to any physical effect, but is purely grid related. This is because the current being drawn by the probe has become comparable to the current across the outer grid boundaries. Therefore the outer grid boundaries do not extend far enough into the plasma for a disk of this size. The other two curves (G equal to 4 and 5.33) show only negligible difference. Since the probe will be larger for $G = 4$ (and thus the statistics will be better for the current collected by the probe) this value of G is chosen when the Debye length of the plasma is equal to one disk radius.

A plasma which has a smaller Debye length will have a more tightly compacted sheath surrounding the probe. This means that a value of $G = 4$ can safely be used for runs which have a Debye length larger than one disk radius. Simulation runs with a Debye length larger than one disk radius would have to be evaluated again in the manner described above in order to find a new value of G.

We will now present the results of simulation runs of a circular planar satellite probe. First one typical run will be studied in detail and the procedure for finding points on the current-voltage characteristic examined. The input parameters for this typical run are given in Table I.

As the simulation run progresses, information which describes the time history of the run is collected and later written to magnetic tape. This tape is then processed on a

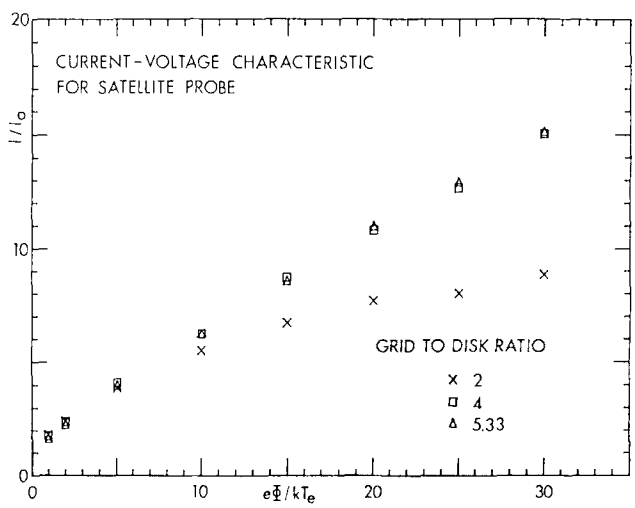

FIG. 3. Current-voltage characteristics for the satellite probe showing the effect of changing the grid to disk ratio.

TABLE I. Input parameters for the example run.

Parameter	Input value
Number of macroparticles of each species	2000
Grid size	32×32
Grid to disk ratio	4
Debye length	1 disk radius
Temperature	1 eV
Voltage on disk	$+10\,e\phi/kT_e$
Proton mass/electron mass	1
Number of time steps	1000

Modcomp II minicomputer. Plots are displayed and the portion of the run in which the simulation plasma is in equilibrium is determined.

An example of such a plot is shown in Fig. 4. This graph shows the number of macroparticles of each species in the system versus time. When the simulation run begins, there are 2000 particles of each species present. The positive voltage attracts macroelectrons and repels macroprotons. The number of macroprotons in the system decreases during the first two hundred time steps because they are leaving the outer grid boundaries at a faster rate than they are entering. The macroprotons are entering the outer grid boundary at a precalculated rate which assumes the outer boundary is at zero potential with respect to the plasma. This is not a valid assumption at the beginning of this run since the electron sheath has not had time to shield the outer plasma region from the probe potential. The number of macroelectrons in the system also decreases. This is due to the macroelectrons being absorbed by the probe and the satellite skin at a faster rate than they enter the outer grid boundary. The presence of the absorbing satellite skin will cause a major decrease in the number of macroelectrons in the system at all voltages. After an equilibrium state has been reached, there are approximately 1500 macroelectrons and 1400 macroprotons in the system for the remainder of the run. The larger number of macroelectrons is accounted for the by the presence of the electron sheath which surrounds the probe.

Figure 5 shows the average kinetic energy of both particle species. The macroelectrons begin the run with an average kinetic energy of about 0.92×10^{-6} ergs/macroelectron. Their kinetic energy begins to increase as the particles are accelerated toward the probe. After the electron sheath has been formed, the kinetic energy for the electrons remains nearly constant at a value of about 0.108×10^{-5} ergs/macroelectron. The macroprotons also experience an increase in average kinetic energy as they are accelerated away from the probe region. As the faster moving macroprotons begin to leave the grid area depleting the system of higher energy protons, the kinetic energy decreases. By this time the electron sheath has begun to form and to shield the outer regions of the grid from the effects of the probe. Thus the kinetic energy of the macroprotons gradually builds back up to what it was at the beginning of the run, to about 0.92×10^{-6} ergs/macroproton.

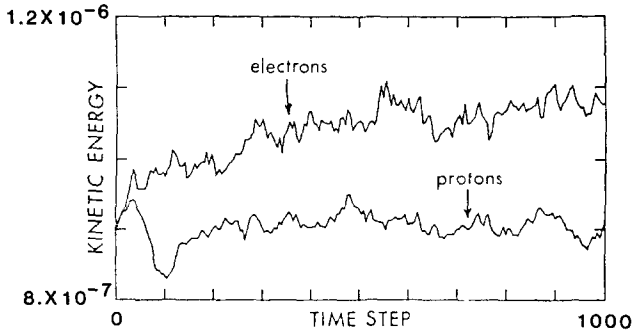

FIG. 5. Average kinetic energy of the macroparticles for the circular planar satellite probe.

Figure 6 is a plot of the average drift energy of the macroparticle versus time. Drift energy is defined to be the square of the vector sum of the individual particle's velocities. Large values of drift velocity mean that the plasma has a directed flow velocity. The average drift velocity of the macroelectrons gradually increases until the sheath has formed and an equilibrium state is reached at about 0.14×10^{-6} ergs/macroelectron. This drift velocity is composed of a small amount of drift by the macroelectrons being accelerated across the sheath region. Also, the absorbing satellite skin will create a drift in the $-z$ direction by removing macroparticles of both species. This accounts for some of the drift for electrons and much of the drift for protons.

The potential energy of the system is shown in Fig. 7. The potential energy at the beginning of the run is slightly positive, due to fluctuations in the initial loading of the macroparticles. Very quickly the potential energy goes to a neg-

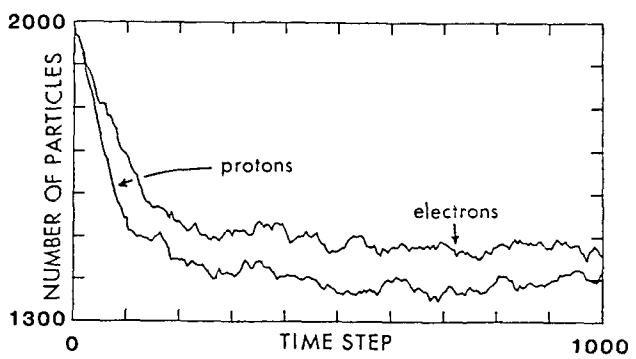

FIG. 4. Number of macroparticles in the system for the circular planar satellite probe.

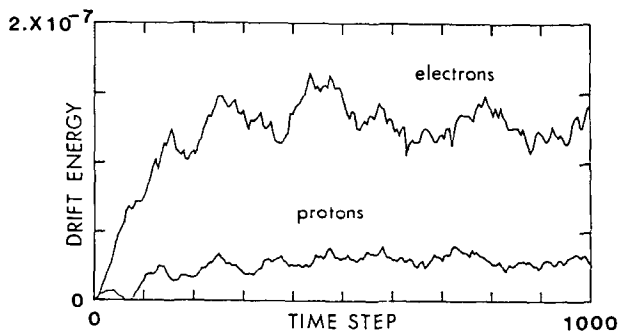

FIG. 6. Average drift energy of the macroparticles for the circular planar satellite probe.

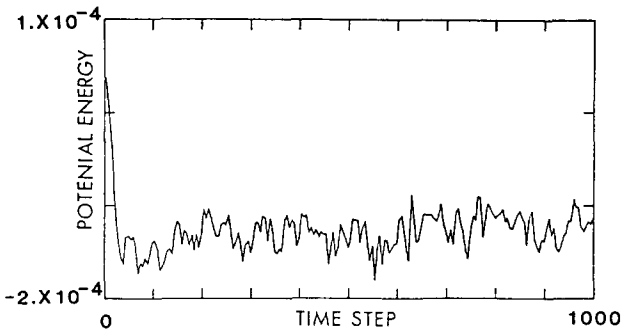

FIG. 7. Potential energy of the system for the circular planar satellite probe.

ative value as the negatively charged electrons form the sheath around the positive probe. A value of about -0.12×10^{-3} ergs is maintained throughout the remainder of the simulation run.

These four plots are used to establish the time when the system reaches an equilibrium state, in this case after 300 time steps. Using another plot of the total number of macroelectrons collected by the probe versus time, a linear least-squares fit was made of the data points between time steps 300 to 1000. This determined the equilibrium current to the probe. For this case, I/I_0 was found to be 6.23.

In order to understand how the formation of the electron sheath affects the potential distribution surrounding the probe, several types of potential plots were developed, two of which are shown in Figs. 8 and 9. Figure 8 is a three-dimensional plot of the potential on the vertical axis versus *r-z* coordinates on the other two axes. The probe in this example is being held at $+10e\phi/kT_e$, while the satellite skin and the outer grid boundaries are held at $0e\phi/kT_e$. The important feature of this plot is that the potential goes to zero well inside the outer grid boundary. This means that the sheath region and the major portion of the transition region are included inside the grid boundaries. Setting the outer grid boundaries to zero potential is therefore justified.

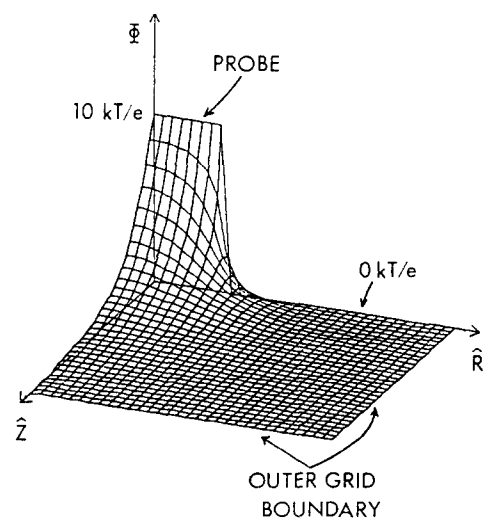

FIG. 8. Three-dimensional plot of the potential for the circular planar satellite probe. Potential is plotted on the vertical axis and the *r-z* coordinates on the other two axes.

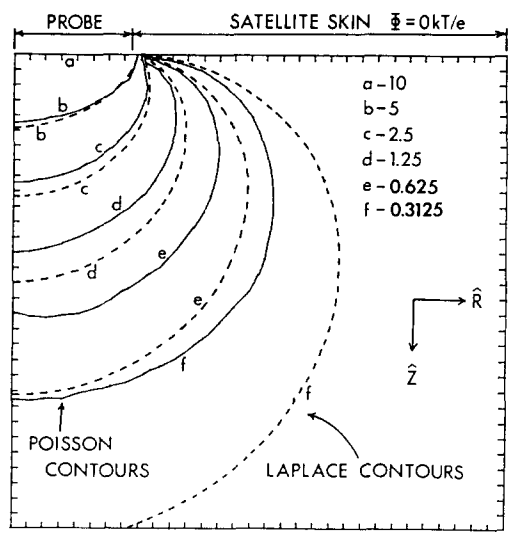

FIG. 9. Potential contour plot for the circular planar satellite probe. The solid lines are contours of the potential distribution shown in Fig. 8. The dashed lines are contours for a Laplace field.

Figure 9 is a potential contour plot. The solid lines are contours of the potential distribution shown as a 3-D plot in Fig. 8. The dashed lines are potential contours for a Laplace field, that is, these are the contours which would exist for the same probe voltage in the absence of a plasma. The Laplace field is given by

$$\phi(r,z)=\phi_0\int_0^\infty e^{-(zt/a)}J_1(t)\,J_0(rt/a)\,dt, \tag{5}$$

where J_0 and J_1 are Bessel functions of the zero and first order. As expected, the sheath causes the contours to be pulled in towards the probe. This plot is in substantial agreement with a contour plot shown by Parker and Whipple[21] for a plasma of Debye length 0.3 times the probe radius.

Enough computer runs of the type described above were made to construct a family of six current-voltage characteristics, each characteristic representing a plasma of different Debye length. In all of these runs, ion mass is equal to electron mass, and ion temperature is equal to electron temperature. Each separate characteristic curve consists of eight separate runs with probe voltages ranging from 1 to 30 $e\phi/kT_e$. These were carried out on a CRAY-1 computer. The average run time to complete one characteristic curve was about 9 min. This family of current-voltage characteristics is shown in Fig. 10. In this figure, the radius of the probe is measured in Debye lengths.

In order to obtain the characteristic curve for an infinite Debye length plasma (zero disk radius), special modifications had to be made in the method of inserting macroparticles across the outer grid boundaries. For an infinite Debye length plasma no sheath is formed, so the plasma particles move in a Laplace field. Therefore, the potential on the outer grid boundaries can no longer be taken as zero for purposes of particle insertion. Since protons are repelled by the positive probe potential, the proper number of protons which cross an area held at a fixed potential can be approximated by the Boltzmann density:

$$n=n_0\exp(-e\phi/kT), \tag{6}$$

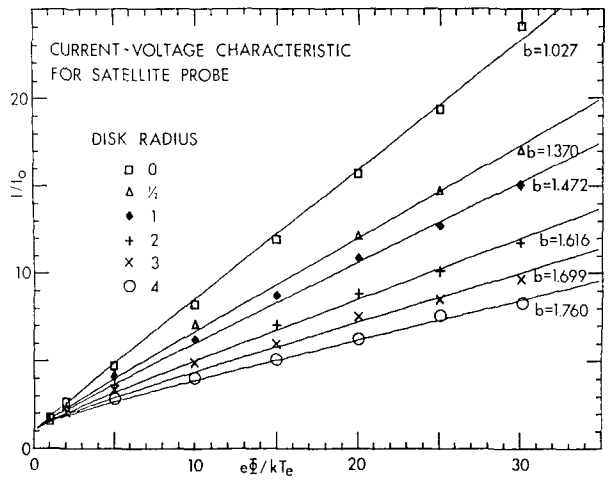

FIG. 10. Current-voltage characteristics for the circular planar satellite probe. Curves for six different plasma Debye lengths are shown. The solid lines are fits of Eq. (7) to each set of points.

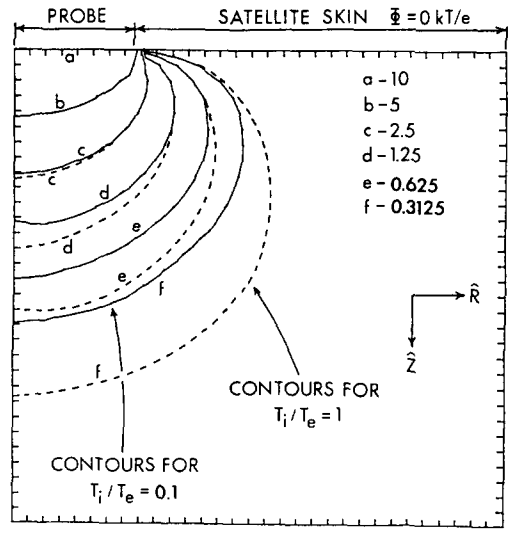

FIG. 11. Potential contour plot for the circular planar satellite probe. The solid lines are potential contours for $T_i/T_e = 0.1$. The dashed lines are potential contours for $T_i/T_e = 1$.

where n is the density of the plasma in a region where the potential is $e\phi/kT$, and n_0 is the density at infinity. This condition is of course not valid near the absorbing satellite skin, but for simplicity, it was used for the entire outer grid boundary region. The Laplace potential varies as a function on the boundary. Thus, a rough estimate is made by finding the average of the Laplace potential on boundary region 4 and again on boundary region 5 (see Fig. 2). These potentials are used in Eq. (6) in order to modify the results of Sec. II. The electron density cannot be approximated by the Boltzmann density since they will have a directed velocity toward the probe. This directed velocity is estimated by using the average potential described above. Both corrections will be small, due to the dipole-like behavior of the satellite probe potential distribution away from the probe. These corrections result in a slightly greater number of electrons than protons being inserted across the outer boundary regions. This simple model produced surprisingly good agreement with theory.

Figure 10 shows that the highest values of I/I_0 can be expected when the Debye length of the plasma is infinite. When the Debye length becomes finite, shielding of the probe begins, and the effective volume from which the probe can collect particles is no longer infinite, but equal to the volume of the sheath. Therefore as the Debye length of the plasma decreases, the current-voltage characteristic curves drop to smaller values of I/I_0.

As pointed out before, the mass ratio does not affect the characteristics for values of $e\phi/kT_i \gg 1$. Changing the temperature ratio of the two species affects the energy and therefore the characteristics will change. Figure 11 is a contour plot of the potential distribution shown before in Fig. 9 compared with the potential distribution of a run with similar parameters except for the temperature ratio, which is $T_i/T_e = 0.1$. The ions, which have less energy, can no longer penetrate as far into the transition region or outer sheath region. This causes the sheath to collapse closer to the probe. Only the outer part of the sheath region is effected, since this is the only region the finite temperature ions can penetrate.

A theory for the circular planar satellite probe has been developed by Parker and Whipple.[21] By studying the effect of excluded trajectories in velocity space they have shown that the current density j at the center of the probe can be given by

$$\frac{j}{j_0} = 1 + \frac{e\phi_0}{kT} - \frac{b^2}{4}\left(\frac{e\phi_0}{kT}\right)^2 \exp\left(\frac{e\phi_0}{kT}\right) E_1\left(\frac{e\phi_0}{kT}\right), \quad (7)$$

where E_1 is the exponential integral

$$E_1(x) = \int_x^\infty e^{-t}\frac{dt}{t}. \quad (8)$$

b is a parameter of order unity which characterizes the potential distribution surrounding the probe. A value of $b = 1$ corresponds to a Laplace field.

A least-squares fit of Eq. (7) was made to the current-voltage characteristics shown in Fig. 10. The characteristic for the Laplace field was found to have a value of $b = 1.027$, remarkably close to the theoretical value of $b = 1$ considering the simple boundary conditions used. A graph of b versus the radius of the probe (in Debye lengths) is shown in Fig. 12.

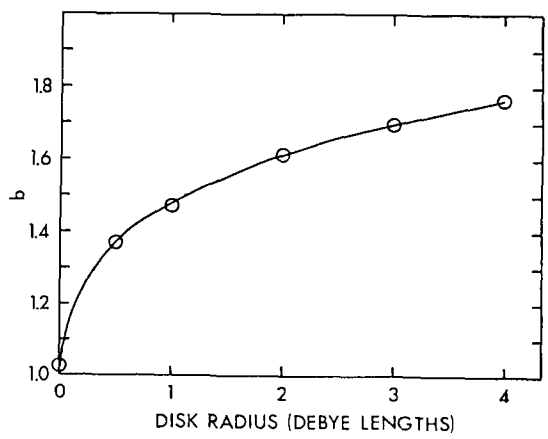

FIG. 12. Graph of the parameter b from Eq. (7) vs disk radius in Debye lengths.

It should be noted that Eq. (7) is a measure of the current density at the center of the probe. Parker and Whipple state that for the Laplace case the current density is fairly constant over the entire probe, but in the Poisson case the current density drops as a function of probe radius. Indeed, the fits of the characteristics other than the Laplace case seem to slightly underestimate the current at the lower voltages while overestimating the current at the higher voltages.

IV. CHARACTERISTICS OF A DISK-SHAPED PROBE

In this section, the configuration will be that of a disk-shaped probe surrounded on all sides by plasma. In this configuration, not only azimuthal symmetry is used, but up-down symmetry above and below the $z = 0$ plane is also employed. This symmetry demands that in boundary region 2 the electric field in the z direction be zero. Therefore, this becomes a mixed boundary value problem in the $z = 0$ plane. Equipotential contours for a vacuum field with the disk will now be much further away from the body of the probe. This in turn implies that more negative charge will be required to shield the positive probe.

Because of the different potential distribution that will exist, the grid to disk ratio G was redetermined. Tests similar to the one shown in Fig. 3 show almost no difference in the characteristics for ratios of 5.33 and 8, so a value of $G = 5.33$ was chosen. For Debye lengths larger than one disk radius, a value of $G = 4$ will suffice.

Current-voltage characteristics were not found for plasmas with a Debye length more than one disk radius. These required a value of $G = 8$, which makes the disk radius only 4 grid cells. As a result too few macroparticles are collected by the probe to obtain smooth characteristic curves.

The results of a typical run will now be considered in order to provide a comparison with those in the previous section. Run parameters are the same as those given before, except that G is now equal to 5.33.

Figure 13 is a plot of the number of macroparticles in the simulation system versus time. The number of macroprotons decreases in the first one hundred time steps because they are being forced out of the system at a faster rate than they are entering. By time step 100 the sheath region has been formed, and the number of protons settles down to an equilibrium value of about 1750. There are more protons in the system at equilibrium than with the satellite probe because there is no absorbing satellite skin region. The absence of this absorbing region also has an effect on the number of macroelectrons in the system. At equilibrium, there are about 1950 macroelectrons in the system.

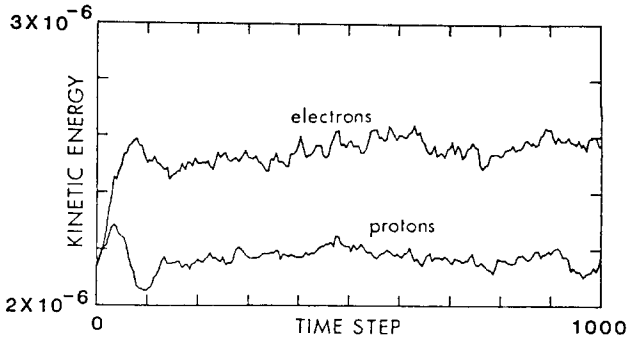

FIG. 14. Average kinetic energy of the macroparticles for the disk-shaped probe.

The average kinetic energy of the macroparticles is shown in Fig. 14. The shape of the curve for macroprotons is the same as for the satellite probe. The macroprotons experience a more rapid rise in energy, due to the unshielded potential extending further out into the grid area at the beginning of the run. After about 100 time steps, the kinetic energy curve decreases as the system is depleted of higher energy particles. This system comes to an equilibrium more rapidly than the satellite probe configuration—after 150 time steps. At equilibrium, the average kinetic energy per macroelectron is about 0.255×10^{-5} ergs/macroelectron and for macroprotons is about 0.215×10^{-5} ergs/macroproton. These cannot be compared directly to the values quoted for the satellite probe. The different grid to disk ratio changes the number of particles represented by a macroparticle. Comparing the average energies of individual particles gives values of 2.8×10^{-12} ergs/electron and 2.4×10^{-12} ergs/proton for both the satellite probe and the disk shaped probe.

A large difference occurs between Figs. 15 and 6, which show the average drift energy of the macroparticles. For the disk, the drift energies of both species rises rapidly as the macroelectrons are accelerated toward the probe and the macroprotons are accelerated away from it. The decrease in drift energy occurs when the electron sheath is formed, and

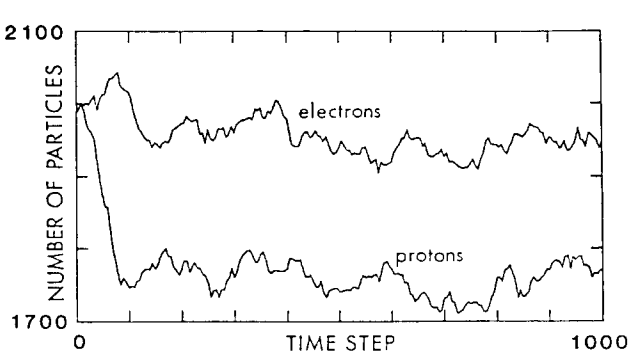

FIG. 13. Number of macroparticles in the system for the disk-shaped probe.

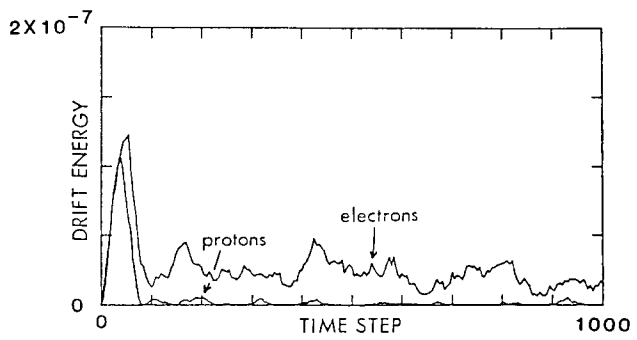

FIG. 15. Average drift energy of the macroparticles for the disk-shaped probe.

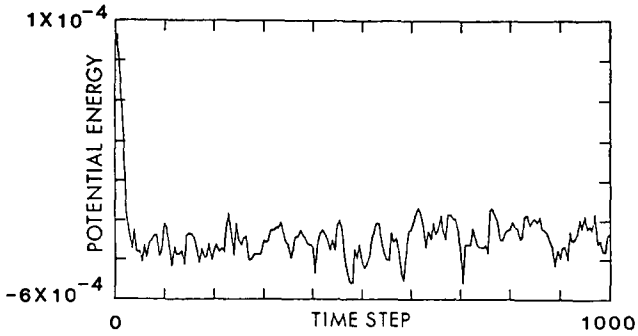

FIG. 16. Potential energy of the system for the disk-shaped probe.

particles in the outer plasma region are no longer accelerated to high velocities, quickly depleting the system of the higher energy particles. The drift energies then fall down to their equilibrium values. The macroprotons have a very small drift in the outer regions of the plasma due to acceleration in the transition region. The macroelectrons have a larger average drift from being accelerated across the sheath region. Referring back to Fig. 6 and the drift velocities for the satellite probe, it can be seen that for this case the major part of the drift is due to the absorbing satellite skin (which removes macroparticles traveling in the $-z$ direction), and is not an effect of the probe.

Figure 16 shows the potential energy of the system versus time. The only difference between this and Fig. 7 is the magnitude of the potential energy at equilbrium. The equilibrium value for the disk is about three times the value for the satellite probe.

The structure of the sheath surrounding the disk-shaped probe is illustrated in the three-dimensional potential plot in Fig. 17. The sheath now surrounds the probe in all directions, the grid size being large enough that the sheath is entirely enclosed well within the grid boundaries. This confirms that a proper grid to disk ratio was chosen.

Figure 18 is a potential contour plot which shows the

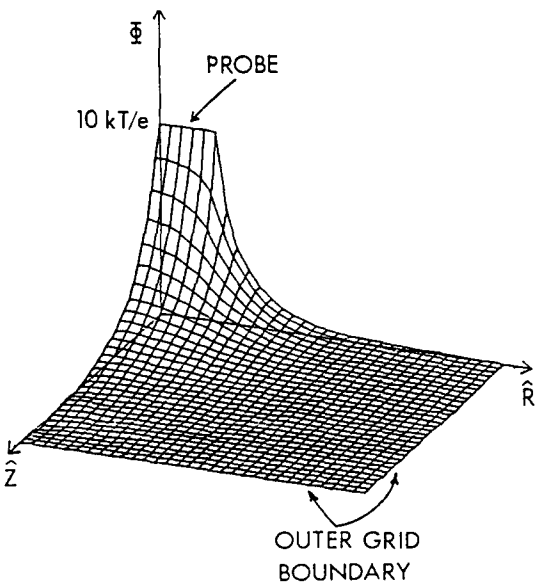

FIG. 17. Three-dimensional plot of the potential for the disk-shaped probe.

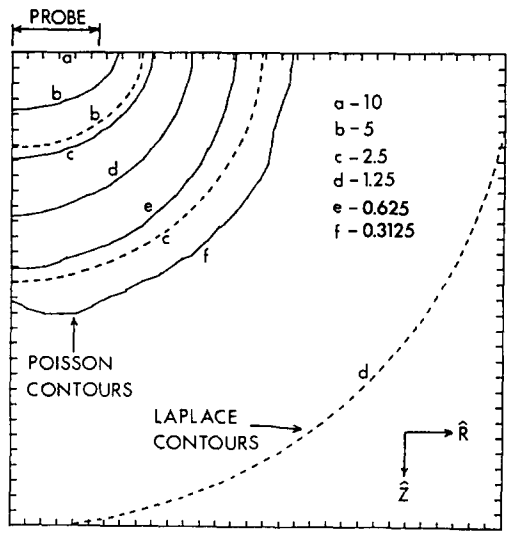

FIG. 18. Potential contour plot for the disk-shaped probe. The solid lines are contours of the potential distribution shown in Fig. 17. The dashed lines are contours for a Laplace field.

difference between Laplace potential contours and Poisson contours. The Laplace contours are sections of oblate spheroids, and these contours extend much further out into the plasma than the Laplace contours for the satellite probe. The shielding behavior is illustrated in Fig. 19. This is a voltage profile of both the Laplace and Poisson potentials in the grid cells parallel and next to the z axis. The potential directly on the z axis is not computed in the simulation. Debye shielding in one-dimension is given by

$$\phi = \phi_0 \exp(-|z|/\lambda_D), \tag{9}$$

where $e\phi/kT_e \ll 1$. It can be seen that the shielding of a disk causes the potential to decrease slightly faster than $\exp(z/\lambda_D)$, where z/λ_D is the distance along the z axis in terms of the Debye length of the plasma. The disk is not an infinite plane, so the shielding distance is shorter than for the one-dimensional case.

Current-voltage characteristics for the disk-shaped probe are shown in Fig. 20. One major difference from the

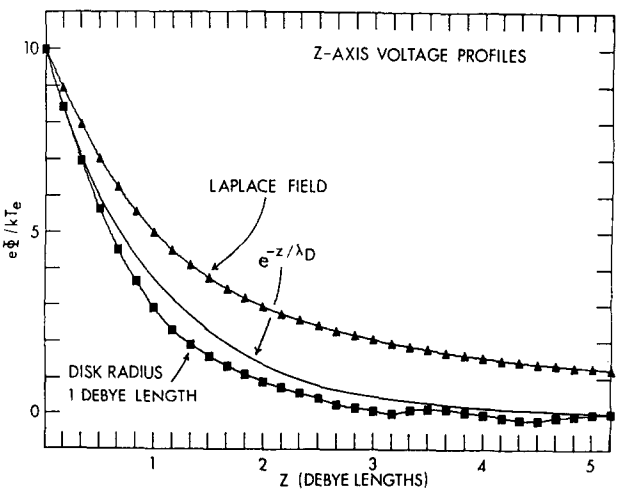

FIG. 19. Voltage profile of the Poisson and Laplace potentials in the grid cells parallel and next to the z axis. Shielding of a disk causes the potential to decrease slightly faster than $\exp(-z/\lambda_D)$.

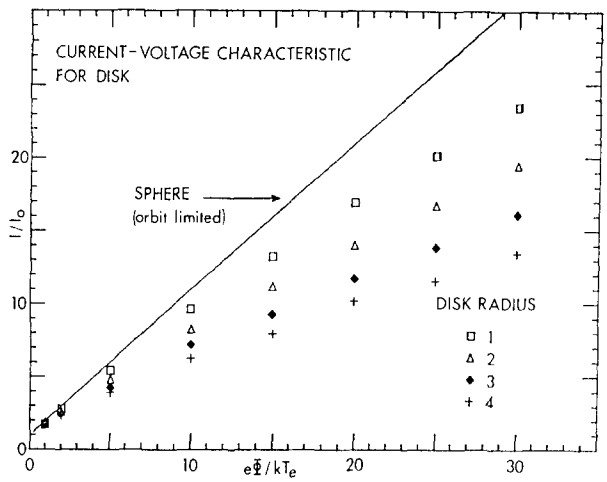

FIG. 20. Current-voltage characteristics for the disk-shaped probe. Curves for four different plasma Debye lengths are shown. The solid line is the characteristic for an orbit-limited sphere.

characteristic curves for the satellite probe is that much larger values of I/I_0 are obtained with the disk. This indicates that the sheath region around the disk is larger than the sheath surrounding the satellite probe. Larger values of plasma Debye length will of course increase the slope of the characteristic. A limiting value can be established by considering the characteristic of an accelerating sphere for the orbit-limited case (infinite Debye length). Laframboise and Parker[20] have shown that oblate spheroids having a major to minor axis ratio less than 2.537 will have the same characteristics in the orbit-limited case as a sphere. A disk has a major to minor axis ratio of infinity, and will be more sensitive to the effects of shielding. It is not surprising that Fig. 20 shows characteristics for the disk lying well below that for a sphere.

V. SUMMARY AND CONCLUSIONS

The purpose of this numerical simulation was to study electron accelerating probe characteristics for the disk-shaped probe. Two different probe configurations were examined: the circular planar satellite probe used by Parker and Whipple in their theoretical study, and the disk-shaped probe entirely surrounded by plasma.

An overall summary of the significant simulation results for the static probe are presented below.

(i) Current-voltage characteristics were presented for the circular planar satellite probe configuration. Plasmas with $T_i/T_e = 1$ and a Debye length ranging from infinity to $\frac{1}{4}$ disk radius were studied. These results were used to obtain a fit of a theoretical equation developed by Parker and Whipple.[21] Figure 12 can be used to obtain an estimate of their theoretical parameter b from which characteristic curves can be generated. Changing the temperature ratio to $T_i/T_e = 0.1$ resulted in the sheath region moving in closer to the probe. Thus, at any given voltage the probe collects less charge for a smaller temperature ratio T_i/T_e.

(ii) Current-voltage characteristics were presented for the disk-shaped probe configuration. Plasmas with $T_i/T_e = 1$ and a Debye length ranging from 1 disk radius to $\frac{1}{4}$ disk radius were studied. More charge was collected by the probe in this configuration as the potential distribution extended further out into the plasma than it did in the satellite probe configuration. Changing the temperature had similar effects to those listed in (i). It was found that the shielding of the disk-shaped probe caused the potential to decrease slightly faster than $\exp(-z/\lambda_D)$ along the z axis.

(iii) In conjunction with some other diagnostic method[40] the current-voltage characteristics given for the two probe configurations can be used to estimate either the plasma density or the temperature of the attracted electrons. The other plasma parameter would have to be supplied by another diagnostic technique.

ACKNOWLEDGMENTS

The authors wish to thank Professor T. P. Armstrong, S. T. Brandon, Dr. R. C. Chaky, and R. Redding for important technical assistance. Invaluable run time on a CRAY-1 computer was provided by United Computing Systems, Kansas City, Missouri. This work was supported in part by NASA Lewis Research Center, Research Grant No. NSG-3290. During 1979-1980, the research by one of the authors (J. H. N.) was supported by a University of Kansas Dissertation Fellowship.

[1]F. F. Chen, in *Pure and Applied Physics*, edited by R. H. Huddlestone and S. L. Leonard (Academic, New York, 1965), pp. 113–200.
[2]J. D. Swift and M. J. R. Schwar, *Electrical Probes for Plasma Diagnostics* (Iliffe, London, 1969).
[3]I. Langmuir, Science **58**, 290 (1923).
[4]I. Langmuir and H. M. Mott-Smith, Gen. Electr. Rev. **27**, 449 (1924).
[5]H. M. Mott-Smith and I. Langmuir, Phys. Rev. **28**, 727 (1926).
[6]L. Tonks and I. Langmuir, Phys. Rev. **34**, 876 (1929).
[7]D. Bohm, E. H. S. Burhop, and K. W. Massey, *The Characteristics of Electrical Discharges In Magnetic Fields* (McGraw-Hill, New York, 1949), Chap. 20.
[8]J. E. Allen and P. C. Thonemann, Proc. Phys. Soc. B **67**, 768 (1954).
[9]J. E. Allen, R. L. F. Boyd, and P. Reynolds, Proc. Phys. Soc. B **70**, 297 (1957).
[10]I. B. Bernstein and I. Rabinowitz, Phys. Fluids **2**, 112 (1959).
[11]S. H. Lam, Phys. Fluids **8**, 73 (1965).
[12]S. H. Lam. Phys. Fluids **8**, 1002 (1965).
[13]J. G. Laframboise, *Rarefied Gas Dynamics*, Vol. II (Academic, New York, 1966).
[14]L. S. Hall and R. P. Freis, Proc. 7th Int. Conf. Phenomena Ionized Gases **3**, 15 (1966).
[15]R. E. Kiel and W. A. Gustafson, Phys. Fluids **9**, 1531 (1966).
[16]R. E. Kiel, AIAA J. **6**, 708 (1968).
[17]R. E. Kiel, AIAA J. **9**, 1380 (1971).
[18]F. F. Chen, C. Etievant, and D. R. Willis, Phys. Fluids **11**, 811 (1968).
[19]B. Nuhn and G. Peter, Proceedings of the 13th International Conference on the Phenomena of Ionized Gases (1977) p. 97.
[20]J. G. Laframboise and L. W. Parker, Phys. Fluids **16**, 629 (1973).
[21]L. W. Parker and E. C. Whipple, Ann. Phys. **44**, 126 (1967).
[22]E. C. Whipple and L. W. Parker, J. Geophys. Res. **74**, 2962 (1969).
[23]L. C. Hale, J. Geophys. Res. **66**, 1554 (1961).
[24]R. E. Bourdeau, E. C. Whipple, J. L. Donley, and S. J. Bauer, J. Geophys. Res. **67**, 467 (1962).
[25]W. B. Hanson, D. D. McKibbin, and G. W. Sharp, J. Geophys. Res. **69**, 2747 (1964).
[26]G. P. Serbu and E. J. R. Maier, J. Geophys. Res. **71**, 3755 (1966).
[27]L. W. Parker and E. C. Whipple, J. Geophys. Res. **75**, 4720 (1970).
[28]N. J. Stevens, F. D. Berkopec, C. K. Pervis, N. Grier, and J. Staskus, AIAA/DGLR 13th International Electric Propulsion Conference Paper 78-672, 1978 (unpublished).

[29]J. H. Nonnast, R. C. Chaky, T. P. Armstrong, J. Enoch, and G. G. Wiseman, USAF/NASA Spacecraft Charging Technical Conference III (1981).
[30]R. C. Chaky, J. H. Nonnast, T. P. Armstrong, J. Enoch, and G. G. Wiseman, USAF/NASA Spacecraft Charging Technical Conference III (1981).
[31]R. C. Chaky, J. H. Nonnast, and J. Enoch, J. Appl. Phys. **52**, 7092 (1981).
[32]F. H. Harlow, Methods Comput. Phys. **3**, 319 (1955).
[33]J. P. Boris, Proc. 4th Conf. Numerical Simulation Plasmas **3**, 3 (1970).
[34]R. L. Morse, Methods Comput. Phys. **9**, 213 (1970).
[35]C. K. Birdsall and A. B. Langdon, *Plasma Physics Via Computer Simulation* (McGraw-Hill, New York, 1982).
[36]R. W. Hockney, Methods Comput. Phys. **9**, 135 (1970).
[37]R. C. Chaky, Ph.D. thesis, University of Kansas (1981).
[38]D. W. Hewett (private communication).
[39]A. B. Langdon and C. K. Birdsall, Phys. Fluids **13**, 2115 (1970).
[40]R. H. Huddlestone and S. L. Leonard, editors, *Plasma Diagnostic Techniques* (Academic, New York, 1965).